IEEE Access
Multidisciplinary ⋮ Rapid Review ⋮ Open Access Journal

Received 12 April 2024, accepted 10 May 2024, date of publication 20 May 2024, date of current version 29 May 2024.

Digital Object Identifier 10.1109/ACCESS.2024.3402659

RESEARCH ARTICLE

A New Hybrid Magnetic Coupler in Inductive Power Transfer System for High Misalignment Tolerance

PENGFEI CAO[1], (Member, IEEE), JIQIANG SHANG[1], ZHENGNAN YUAN[1,2], MING SONG[1], CONGCONG LI[1], PENGCHENG FU[1], ZHONGXIU HAO[1], YONG YANG[3], AND ANZONG HU[4]

[1]School of Information Science and Engineering, Lanzhou University, Lanzhou 730000, China
[2]Lanzhou Institute of Physics, Lanzhou 730000, China
[3]Department of Industry and Information Technology of Gansu Province, Lanzhou 730000, China
[4]Lanzhou Huayu Aerospace Service Guarantee Company Ltd., Lanzhou 730000, China

Corresponding authors: Pengfei Cao (caopf@lzu.edu.cn) and Anzong Hu (316351432@qq.com)

This work was supported in part by the Natural Science Foundation of Gansu Province (No. 20JR10RA614, 22YF7GA182), the National Natural Science Foundation of China under Grant 61804071, the Open Fund of Key Laboratory of Time and Frequency Primary Standards, Chinese Academy of Sciences (CAS), the Gansu Provincial University Industry Support Plan Project (2022CYZC-07 2022), and the Lanzhou Chengguan District Science and Technology Plan Project (2021RCCX0031).

ABSTRACT Wireless charging has become increasingly popular in low and medium-power applications, such as motor-driven carriers, unmanned aerial vehicles, electric bicycles, and inspection robots. Nevertheless, pad misalignment can significantly affect the system performance, leading to higher losses and a reduction in the power output. Particularly in the all directions of anti-misalignment strategies, a greater number of inverters and compensations are necessitated, leading to increased system dimensions and heightened complexity. This article proposes a new hybrid coupler that only uses a bipolar pad as the secondary pad and a solenoid (S coil) with an added quadrature coil (Q coil) as the primary pad. We develop and test a 50W prototype in the laboratory. The size of the coupler is 355 mm × 290 mm. The experimental and simulation results demonstrate that when the distance between the transmitter and receiver is 60 mm, the transmission efficiency remains within a range of 72% to 90% for all directions of anti-misalignment, while the output voltage exhibits fluctuations within a margin of 10%. The results indicate that the coupler has a great potential for use in low and medium power applications, and can even be used in high-power equipment.

INDEX TERMS Inductive power transfer (IPT), magnetic coupler, pad misalignment, solenoid-quadrature coil.

I. INTRODUCTION

Inductive Power Transfer (IPT) technology has recently emerged as a prominent solution in a variety of application domains, including the provision of power to eddy current non-destructive testing (ECNDT) sensors [1], [2], [3], [4]. However, the technology faces challenges due to the inevitable deviations between the receiver and transmitter, leading to a reduction in transmission efficiency. One of the key factors impacting the performance and reliability of IPT systems is the misalignment of the pads between the receiver and the transmitter. This misalignment causes variations in mutual inductance, resulting in significant fluctuations in output voltage/current and increased power losses. Therefore, enhancing the tolerance to misalignment is a critical objective in the further development and optimization of IPT technology.

In recent years, a variety of strategies have been developed to address the misalignment issue in inductive power transfer (IPT) systems [5]. For instance, the wireless charging

The associate editor coordinating the review of this manuscript and approving it for publication was Su Yan.

efficiency of e-cycles can be enhanced through the refinement of the series-series (SS) compensated design [6]. Broadly speaking, the solutions to the misalignment problem fall into two main categories: optimization of compensation topologies and modification of magnetic couplers.

The first category involves methods related to compensation topologies, which include control strategies and compensation of circuit topologies. One approach is to enhance efficiency by incorporating a control circuit that adjusts the working frequency and voltage phase during misalignment. Techniques such as phase-shift modulation in full-bridge converters [7], [8] and duty cycle control in dc-dc converters [9], [10], [11] have been shown to mitigate power loss due to misalignment. Another approach involves varying circuit compensation topologies to bolster misalignment tolerance. In this context, a combination of LCL-LCL and S-S compensations has been employed to maintain steady output power despite pad misalignment [12], [13], [14], [15]. However, refining compensation topologies may introduce additional resonant elements, potentially diminishing the system's overall effectiveness [16].

The second category focuses on the design of magnetic couplers (MCs), such as the flat solenoid coupler (FSC) [17], double-D (DD) [18], DD quadrature (DDQ) [18], and bipolar (BP) [19]. Each of these MCs offers unique advantages and limitations. The FSC, for example, can withstand significant pad misalignment along the winding direction and generate a more substantial magnetic field compared to single-sided winding structures. Nevertheless, its tolerance for misalignment perpendicular to the winding is limited [20], [21], [22]. To overcome this challenge, a DD coil with a magnetic core has been proposed. However, this design encounters a zero-coupling point (ZCP) when misaligned along the longitudinal direction of the magnetic core, leading to a significant drop in transmission power and compromised system performance in that direction.

The Quadrature coils (Q coils) were proposed to address the zero-coupling point (ZCP) issue, but they exhibit a low coupling coefficient and lack experimental data on performance in various misalignment directions [23]. DDQ coils, combining Q coils with double-D (DD) coils, offer a solution to the ZCP problem, yet require extensive copper wire winding, increasing losses. The Bipolar Pad (BP) coil provides a more efficient use of copper wire, achieving similar misalignment tolerance to the DDQ coil but with a lower magnetic field intensity due to its single-sided double-winding structure. Reconfigurable structures like multicoil schemes enhance tolerance to deviations in any direction but necessitate numerous selection switches and components, leading to higher costs, power losses, and spatial requirements [24], [25], [26], [27], [28]. In designing magnetic coupler coils, factors such as misalignment tolerance, coupling coefficient, structural complexity, and cost must be carefully considered [29]. Consequently, magnetic coupler schemes present several design and optimization challenges:

1. The optimization of the magnetic core's shape and size, along with the implementation of appropriate magnetic shields, is crucial for enhancing the coupling coefficient. While modified flat solenoid couplers (FSCs) [30], [31], [32], [33], [34], [35] can reduce the quantity of magnetic cores, thereby lowering weight and cost, their tolerance to deviations along the magnetic field direction remains relatively unchanged [36].
2. Magnetic coupler structures, such as double-D (DD), DD quadrature (DDQ), and bipolar (BP) designs, offer increased tolerance to pad misalignment in specific directions but fail to provide comprehensive coverage in all directions, including x, y, z, diagonal and rotational axes. Multiple coil configurations, including DD and double-sided decoupled coils, demonstrate improved performance in multi-directional misalignment tolerance. However, these configurations necessitate additional inverters and devices, such as numerous LCL-LCL and S-S compensations, leading to increased size and system complexity [37], [38], [39], [40]. Furthermore, the close placement of these coils results in multiple cross-coupling coefficients, complicating the design parameters [41].

To tackle these challenges, we have developed an innovative hybrid magnetic coupler design. The primary pad of this coupler features a solenoid coil (S coil) integrated with a quadrature coil (Q coil), collectively termed as SQ. Additionally, the design of the magnetic core in this structure is oriented perpendicular to the winding direction of the S coil. For the secondary pad, we utilize a bipolar pad (BP) to effectively capture both the parallel and perpendicular magnetic flux generated by the primary SQ pad.

This innovative design addresses two key issues: First, the evenly distributed magnetic core within the entire S coil not only improves the coupling coefficient, but can also better increase the misalignment tolerance along the direction of the magnetic core. In addition, the SQ coils use the same set of magnetic cores to reduce the total number of magnetic cores and the associated cost. What's more, although the SQ-SQ coils can produce a strong vertical magnetic flux, its high magnetic leakage can impair the system's energy transmission efficiency. Thus, it needs to be coupled with different types of coils. Compared with the SQ-SQ type structure in our previous work [42], the SQ-BP structure can reduce the magnetic flux leakage along the misalignment directions because the BP coil can produce a parallel magnetic flux. Besides, compared with the BP-BP type structure (single winding coil structure), the transmitting coil and the solenoid coil (S) have stronger magnetic field in the vertical direction. Therefore, the SQ-BP coils can generate a highly coupled magnetic field, compensating the magnetic flux to prevent ZCPs when there is a misalignment along the vertical winding direction. As a result, this coupling structure can improve the tolerance to misalignment. Therefore, the Issue 1 is solved.

Secondly, our prior research [42] has demonstrated that the Q coil and S coil are decoupled, allowing for independent

treatment. Notably, there is no cross-coupling coefficient between the S and Q coils, simplifying the design process. We only need to consider two types of cross-coupling coefficients: S-BP and Q-BP. Compared to multiple coil designs [37], [38], [39], [40], the SQ-BP configuration boasts a simple and non-periodic structure, resulting in fewer coils, driving circuits, and cross-coupling coefficients. Furthermore, it exhibits superior tolerance to pad misalignment in various directions, including x, y, z diagonal, and rotational. Notably, references on misalignment tolerance in diagonal and rotational directions are scarce. In our design, four straightforward coils and a few circuits effectively address the multi-directional deviation problem, thus solving Issue 2.

A structural analysis is conducted to showcase the mutual inductance of the SQ-BP hybrid coupler, complemented by theoretical analysis and experiments to validate our findings. Subsequently, the misalignment-tolerant performance of the SQ-BP structure is tested and compared with other magnetic couplers. The proposed SQ-BP structure not only boasts a smaller volume and fewer magnetic cores but also exhibits high misalignment tolerance in all directions, including diagonal and rotational, aligning with the specifications of SAE J2954 [43].

The remainder of this article is structured as follows: Section II delves into the operating principles and anti-misalignment characteristics of the SQ-BP hybrid coupler. Section III presents the experimental results of the SQ-BP hybrid coupler within LCL-S compensation networks of the IPT system to validate our proposed method. Section IV provides a conclusion to the article.

II. THEORETICAL ANALYSIS OF THE SQ-BP COUPLER

The circular coil's magnetic field distribution is uniform, maintaining consistent intensity throughout. However, it lacks directional compensation capabilities. In contrast, the rectangular coil exhibits a non-uniform magnetic field distribution, with varying strengths across different regions, allowing for effective compensation under offset conditions through the superposition of multiple coils. Therefore, this study adopts a rectangular coil design. The quadruple pad (QP) structure, analyzed in [23] and [44], is depicted in Figure 1(a), showing the primary pad (SQ) comprising an S coil and a Q coil, with the BP as the secondary pad. Figure 1(b) presents the overall proposed structure, where the Q coil, located below the S coil, is magnetically isolated from it, enabling independent treatment of the two coils.

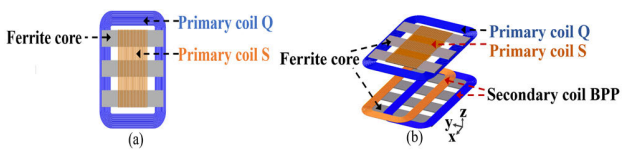

FIGURE 1. Proposed pad structures. (a) Primary pad structure. (b) SQ-BP 3-D model.

The S and Q coils are decoupled, as illustrated in Fig. 2. This decoupling arises because S coils produce parallel flux while Q coils generate perpendicular flux, making it challenging to achieve magnetic coupling between the two coils through their centers. This conclusion is further supported by the mutual inductance between the SQ coils observed in subsequent simulations and experiments. In the illustrations, dots and crosses indicate the direction of current flow, with dots representing current flowing out of the wire and crosses indicating current flowing into the wire. The magnetic field can be enhanced by placing ferrite cores near the SQ and BP. The S coil is wound around the core, which is positioned between the S-Q coils, and the cores should be evenly distributed. The length of the magnetic core extends beyond the edge of the Q coil. In this configuration, the Q coil is enveloped by cores, enhancing the coil coupling strength. The BP coils consist of two separate coils and other components. In the area where the two coils overlap, the currents in the coils flow in opposite directions, while the magnetic field remains in the same direction. This arrangement reduces magnetic field loss and leakage, thereby improving transmission efficiency [24], [25], [26], [27].

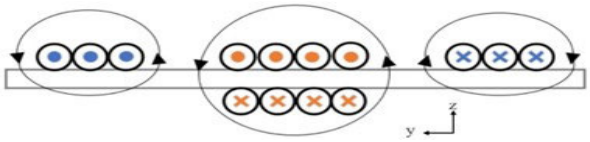

FIGURE 2. SQ coil structure and its associated magnetic field shape.

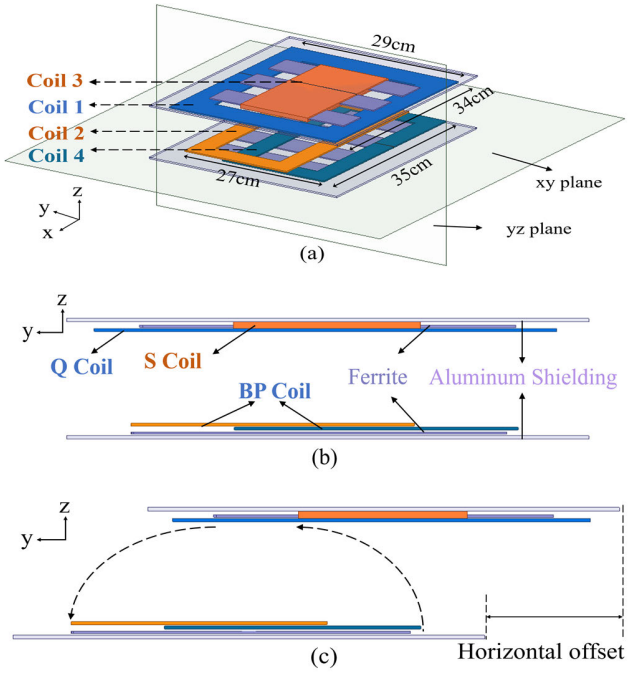

FIGURE 3. (a) Transmitter and receiver with reference axes. (b) Align the receiving and transmitting coils. (c) Receiver has a y-direction misalignment.

Fig. 3 illustrates the operational schematics of the proposed coupling structure, detailing how the coupler functions. In this structure, coils Q (Coil 1) and S (Coil 3) act as the

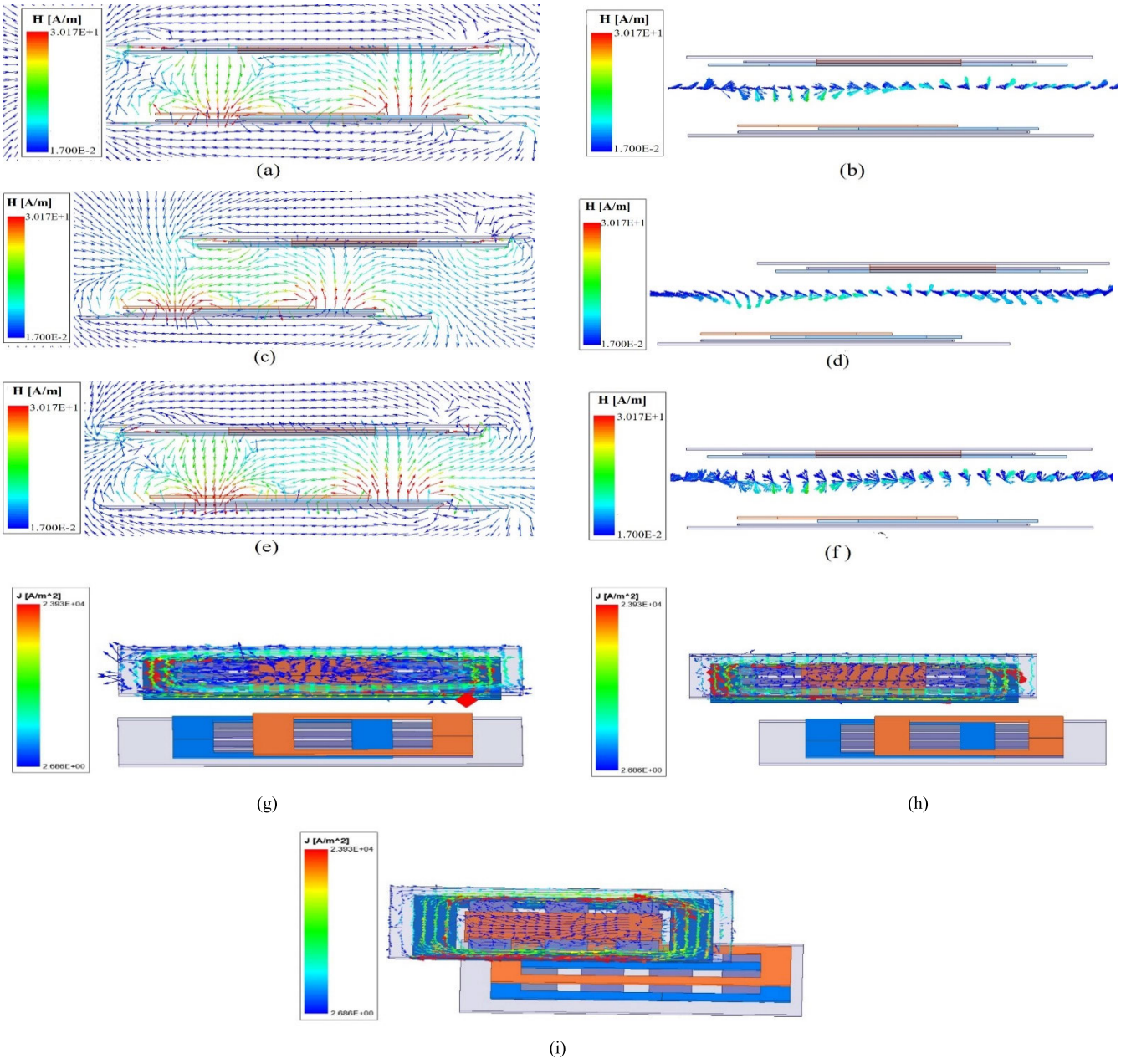

FIGURE 4. Vectors of magnetic flux density (VMFD) in the yz plane and xy plane and the current density vectors in xz and yz of a SQ-BP system. (a) Transmitter and receiver with reference axes that are horizontally aligned (VMFD in the yz plane). (b) Transmitter and receiver with reference axes horizontally aligned (VMFD in the xy plane). (c) Misaligned with a δ_y of 100 mm (VMFD in the yz plane). (d) Misaligned with a δ_y of 100 mm (VMFD in the xy plane). (e) Misaligned with a δ_x of 80 mm (VMFD in the yz plane). (f) Misaligned with a δ_x of 80 mm (VMFD in the xy plane). (i) Transmitter and receiver with reference axes horizontally aligned (current density vectors in the yz plane), (j) Misaligned with a δ_y of 100 mm (current density vectors in the yz plane) and (k) Misaligned with a δ_x of 80 mm (current density vectors in the xz plane).

primary side, while the BP coils (Coils 2 and 4) are on the secondary side, as depicted in Fig. 3(a). The cross-sectional view along the yz plane with horizontal alignment is presented in Fig. 3(b), and a scenario of horizontal misalignment is shown in Fig. 3(c). When the BP pad aligns precisely with the SQ pad, Coil 3 experiences the sole net flux, as indicated in Fig. 3(b). However, when the BP pad is shifted along the y-axis, which is the longitudinal direction of the magnetic core, the net flux through the S coil diminishes, whereas the net flux through the Q coil escalates, as illustrated in Fig. 3(c). Notably, there can be a situation where no net flux passes through the S coil, identified as a zero-coupling point (ZCP), while the Q coil experiences maximum net flux.

To validate the proposed concept, Fig. 4 showcases a magnetic flux density vector diagram from a MAXWELL simulation with a 60 mm air gap, using copper for the coil material and ferrite for the magnetic core. The simulation accounts for eddy currents and is set to a frequency of 100 kHz to replicate real-world conditions. Coil1 generates

a magnetic field perpendicular to the y-axis, while coil3 produces a field parallel to the y-axis. The BP coil consists of two independent coils, coil2 and coil4, which form non-overlapping regions on the left and right sides and overlapping regions in the middle. When the SQ and BP are perfectly aligned, as shown in Fig. 4(a) and (b), the magnetic field directions in the non-overlapping regions of the BP coil are opposite, reducing the sum of the magnetic field generated by the BP coil and the magnetic flux entering coil1, leading to weaker coupling performance. This is based on the principle that the flux entering a coil must equal the flux exiting the coil, as demonstrated in Fig. S1 (a)-(d) in the Supplementary Document Section I. Additionally, the magnetic field vector in the overlapping area of the BP coil is parallel to the y-axis, primarily generated by coil3. Therefore, in the case of perfect alignment between SQ and BP, the coupling predominantly occurs between coil3 and the BP coils. However, when there is a deviation between SQ and BP along the y-axis direction, as seen in the comparison between Fig. 4(c) and Fig. 4(a), the parallel magnetic field vector along the y-axis between the SQ coil and the BP coil decreases, indicating a weakening of the coupling between coil3 and the BP coil. Conversely, if SQ and BP are misaligned in the x-axis direction, as shown in the comparison between Fig. 4(e) and Fig. 4(a), the y-axis parallel magnetic field vector between the SQ coil and the BP coil remains relatively unchanged, maintaining the coupling primarily between coil3 and the BP coil.

Figures 4(c) and (d) illustrate the magnetic flux changes when there is a longitudinal misalignment along the y-axis with respect to the receiver. The magnetic flux through the S coil decreases, while the net magnetic flux through the Q coil increases. This scenario shows that the magnetic flux interaction between the BP coil and Coil 1 compensates for the flux change between Coil 3 and the BP coil, as further supported by the distribution of current density vectors in Figures 4(i)-(k). Similar results are observed for misalignments in diagonal directions, with detailed distributions presented in Section II of the Supplementary Document (Fig. S2). Figures S2(e) and (f) in the Supplementary Document demonstrate that the magnetic flux through the S coil is still reduced with lateral misalignment along the x-axis. Notably, Coil 1 and the BP coil are not coupled during x-direction misalignment processes because the flux-in equals the flux-out between Coil 1 and the BP coil. Figures S2(n)-(p) in the Supplementary Document show that the current density of Coil 1 starts to increase and provide compensation when the rotation angle reaches 20°. As the rotation angle approaches 50°, the overlapping area between the transmitting and receiving coils decreases, leading to a reduction in the current density of Coil 1 and subsequently diminishing the compensation effects. The variations in the coupling coefficient for these cases are presented in Fig. S3 in Section III of the Supplementary Document. A decoupling state is observed between coils on the same side, with the coupling coefficients k_{13} and k_{24} being close to zero.

III. SIMULATION AND EXPERIMENTAL RESULTS OF MISALIGNMENT-TOLERANT PERFORMANCE

A. SIMULATION AND EXPERIMENT ANALYSIS OF SQ-BP COUPLER

To minimize skin effect losses, the proposed SQ-BP coils are constructed using a 320-strand AWG-38 Litz wire. The number of turns for Coils 1 and 3 are 11 and 19, respectively, while Coils 2 and 4 each have 11 turns. Ferrite cores are employed in the SQ-BP to shape and concentrate the magnetic field, with each core measuring 50 mm × 250 mm. The dimensions of the SQ coupler are 355 mm × 290 mm, and the BP coupler measures 344 mm × 275 mm, as depicted in Fig. 5. The use of aluminum plates beneath the coupling structures helps eliminate leakage flux. The effect of aluminum plates, including mutual coupling analysis, is detailed in Figures S4-S6 in Sections IV and V of the Supplementary Document. The positioning and length of the ferrite cores (FC) are analyzed in Section V of the Supplementary Document (Figures S7-S10). Fig. 5 illustrates the structure and dimensions of the SQ-BP.

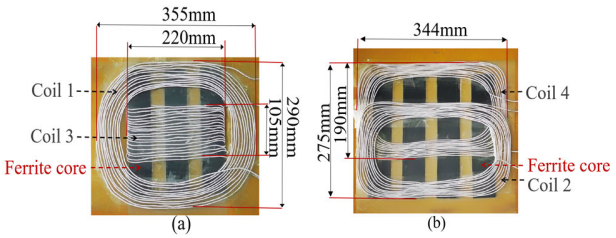

FIGURE 5. Coil structure. (a) Transmitter SQ. (b) Receiver BP.

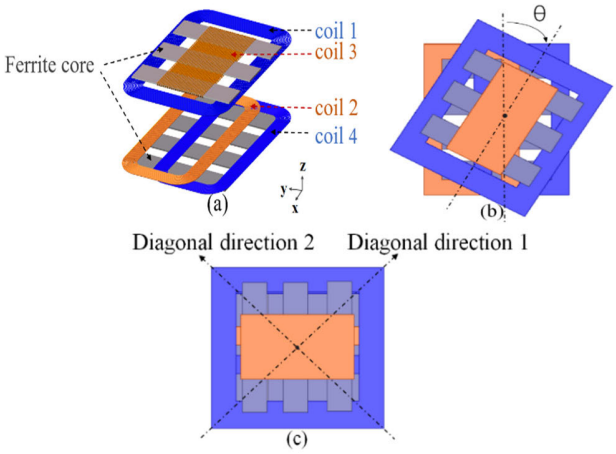

FIGURE 6. Misalignment direction diagram. (a) lateral (x), longitudinal (y), vertical (z), (b) angular, and (c) diagonal directions.

The anti-misalignment performance along the x- and y-directions differs due to the asymmetry between the SQ and BP couplers. As depicted in Fig. 6, this article evaluates misalignments in horizontal/vertical, diagonal, and rotational directions. In these scenarios, Coils 2 and 4 (BP) are displaced in the specified direction.

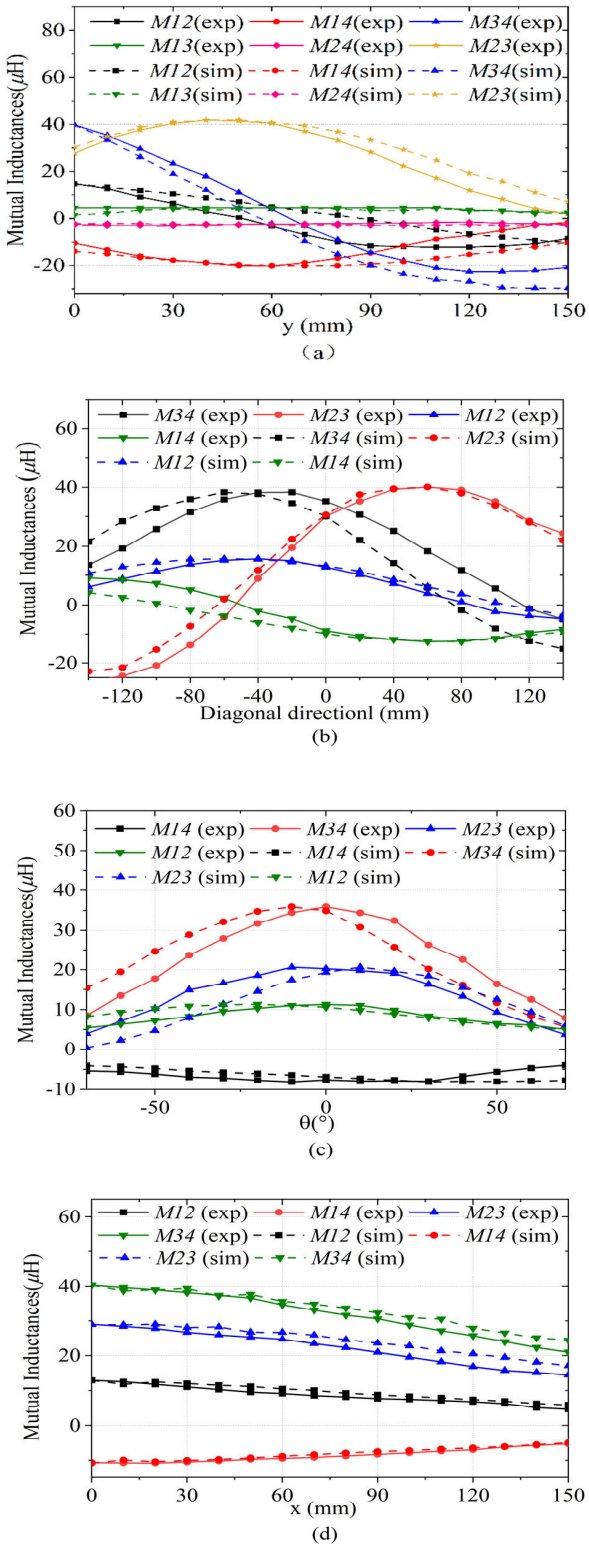

FIGURE 7. A four-way misalignment affects mutual inductances. (a) longitudinal misalignment (*y*- direction), (b) diagonal direction 1 misalignment, (c) angle misalignment, (d) lateral misalignment (*x*- direction).

The mutual inductances between the coils of the SQ-BP structure are indicative of its coupling mechanism. Fig. 7 presents both simulated and experimentally measured variations in mutual inductances for each pair of coupled coils, corresponding to the misalignment directions illustrated in Fig. 6. The associated coupling coefficients follow the same trend as the mutual inductances and are depicted in Fig. S3 in Section III of the Supplementary Document due to space constraints. In the simulation, the mutual inductance can be directly obtained from the MAXWELL software. For experimental measurement, an inverter is used to supply an alternating current of 100 kHz to the primary coils, recording the current I_1. Subsequently, the open circuit voltage U_2 in the secondary coils is recorded to calculate the mutual inductance between the coils using the formula $M = U_2/(\omega I_1)$. It is crucial to ensure that the other coils are inactive when measuring the mutual inductance of a specific pair of coupling coils. Equation (1) establishes that mutual inductance is related to magnetic flux. The study also explores the magnetic field distribution for each pair of coupled coils, with detailed information provided in Section I, Fig. S1 of the Supplementary Document.

Fig. 7 illustrates that only $M23$, $M12$, $M14$, and $M34$ exhibit significant changes with the misalignment directions mentioned above, while $M13$ and $M24$ are small enough to be neglected. This is because the coils on the same side (Coils 1 and 3, and Coils 2 and 4) are decoupled, which aligns with the theoretical analysis. Given the current direction shown in Fig. 2, the mutual inductance value of Coil 12 is opposite to that of Coil 14. Due to the asymmetrical shapes of the manually wound coils, the differing inductance values of Coils 2 and 4 result in the absolute values of $M12$ and $M14$ differing at the pad alignment position. Consequently, when the pad is precisely aligned, the total coupling mutual inductance of Q-BP is nearly zero, confirming the earlier theoretical analysis. However, it is crucial to note that while the total net flux through the Q-BP is zero, the net flux through individual Coil 12 or Coil 14 is not zero, as shown in Fig. S1 (a, b) and (c, d) in Section I of the Supplementary Document.

$$M_{ab} = \Phi_{ab}/I_a \tag{1}$$

As depicted in Fig. 7(a), there is a noticeable discrepancy between the main coupled inductances ($M12$, $M34$) and the cross-coupled inductances ($M23$, $M14$) when misaligned in the *y*-direction. Notably, zero-coupling points (ZCPs) are present in the main coupled mutual inductances ($M12$, $M34$), with the underlying reason discussed in Section VI of the Supplementary Document. Additionally, the cross-coupled mutual inductances ($M23$, $M14$) exhibit relatively large values at the ZCPs. $M34$ becomes zero at the ZCP as the rectangular-ambulatory-plane coils align, as illustrated in Fig. S1(e) and (f) in the Supplementary Document. At the ZCP, the net flux through Coil 12 is zero due to the combined effects of the misaligned Coil 2 and the continuous strip of ferrites, as shown in Fig. S1(g) and (h). Similarly, Coils 14 and 23 experience non-zero flux at the ZCPs. Beyond the ZCP, $M34$ increases again due to repeated

misalignment of Coil 34 and the non-zero magnetic flux through the S coil, as demonstrated in Fig. S1(i) and (j).

A continuous strip of ferrites contributes to an increase in $M12$ after the ZCP [15], as demonstrated in Fig. S2(k) and (l) of the Supplementary Document. In the case of misalignment along the y-axis, it can be concluded that Coils 14 and 23 exhibit mutual inductances that compensate for Coils 12 and 34. This compensation helps maintain a certain misalignment range for the total mutual inductance of the system, aligning with the trends of SQ-BP magnetic flux as shown in Fig. 3(c) and Fig. 4(c) and (d). Fig. 7(b) illustrates the variations in mutual inductance in diagonal directions. Similar to the misalignment process in the y-direction, the single transmitter coil and receiver coil revert to misalignment after alignment, causing the mutual inductance to change from increasing to decreasing. Given that diagonal directions 1 and 2 are treated symmetrically, diagonal direction 2 can be omitted in cases where the change in mutual inductance for the diagonal direction is consistent.

Fig. 7(c) depicts the changes in mutual inductance when angular misalignment occurs between the transmitter and receiver. The mutual inductance exhibits a descending trend due to changes in the magnetic flux between the coils. As the angle of misalignment increases, the net flux between the transmitter and receiver decreases. Fig. 7(d) demonstrates that misalignment along the x-axis reduces the flux through the S-BP and decouples the Q-BP, leading to reduced mutual inductances. The trends of total mutual inductances in the x- direction align with the trends of the SQ-BP magnetic flux, as indicated in Fig. 4(e) and (f). In conclusion, the results suggest that the coupling between Q-BP compensates for the change in mutual inductance between S-BP when misalignment occurs along the longitudinal (y) and diagonal directions, thereby stabilizing power throughput. However, the tolerance to misalignment in the x-axis and angular directions is slightly lower.

B. EXPERIMENTAL ANALYSIS OF THE SQ-BP WITH IPT SYSTEM

Fig.8 and Fig.9 depict the schematic and physical prototype of the circuit structure, respectively, with the relevant parameters listed in Table 1. The experimental setup includes a voltage source (A-BF SS-6010KD), a digital bridge (Victor 4090C), and an oscilloscope (TBS1102B). To enhance vertical misalignment-tolerant performance, the system incorporates a combination of inductor–capacitor–inductor (LCL) and capacitor–inductor (CL) compensation networks [43], achieving high 3-D misalignment-tolerant performance. The analysis of the LCL circuit is provided in Section VII of the Supplementary Document. Additionally, the analysis of misalignment performance in the z-direction is included in Section VII of the Supplementary Document, Figures S15-S16. The efficiency of the system can be calculated using equation (2), with the relevant derivations available in Section VIII of the Supplementary Document. Due to equipment limitations, the input voltage value selected for this experiment is 30.38 V.

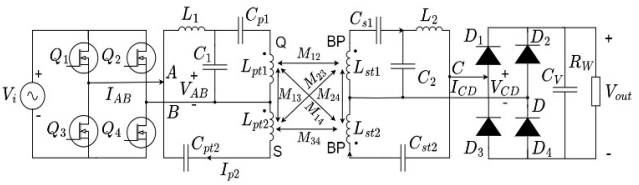

FIGURE 8. Schematic diagram of the overall circuit topology.

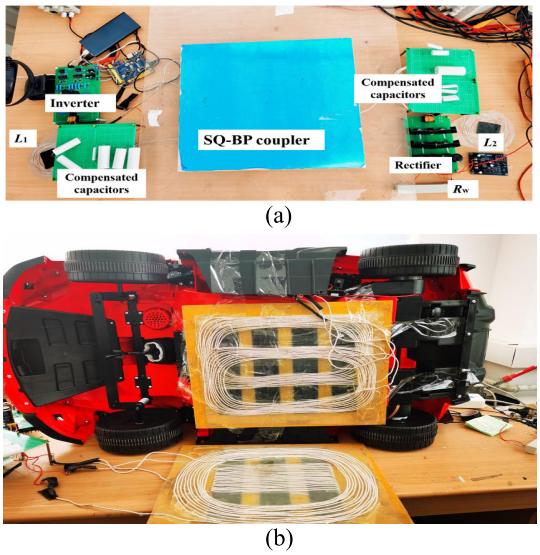

(a)

(b)

FIGURE 9. (a) Prototype's experimental setup. (b) Motor-driven carriers charging device.

TABLE 1. IPT system parameter.

System Parameter	Parameter Value	System Parameter	Parameter Value
f	100 kHz	L_{pt2}	120 μH
R_w	10 Ω	L_{st1}	69.28 μH
V_{in}	30.38 V	L_{st2}	64.5 μH
L_{pt1}	42.3 μH	C_1	115 nF
C_{p1}	119.7 nF	C_{s1}	54 nF
C_{pt2}	21 nF	C_2	115 nF
C_{st2}	42 nF	L_1	22.12 μH
L_2	21.899 μH		

$$\eta = \frac{(V_{out})^2}{R_w} / P_{in} \tag{2}$$

Fig.10 presents the experimental output and input current/voltage waveforms of the inverter and the rectifier for both well-aligned and x-direction misaligned cases. The AC voltages across the inverter and the rectifier are represented by V_{AB} and V_{CD}, respectively, while currents I_{AB} and I_{CD} are measured across the inverter and rectifier, respectively. Further details can be found in the Supplementary Document. To estimate the voltage and current phase angle (PA), a storage device can be employed to read voltage, current, and time information from the oscilloscope as text data.

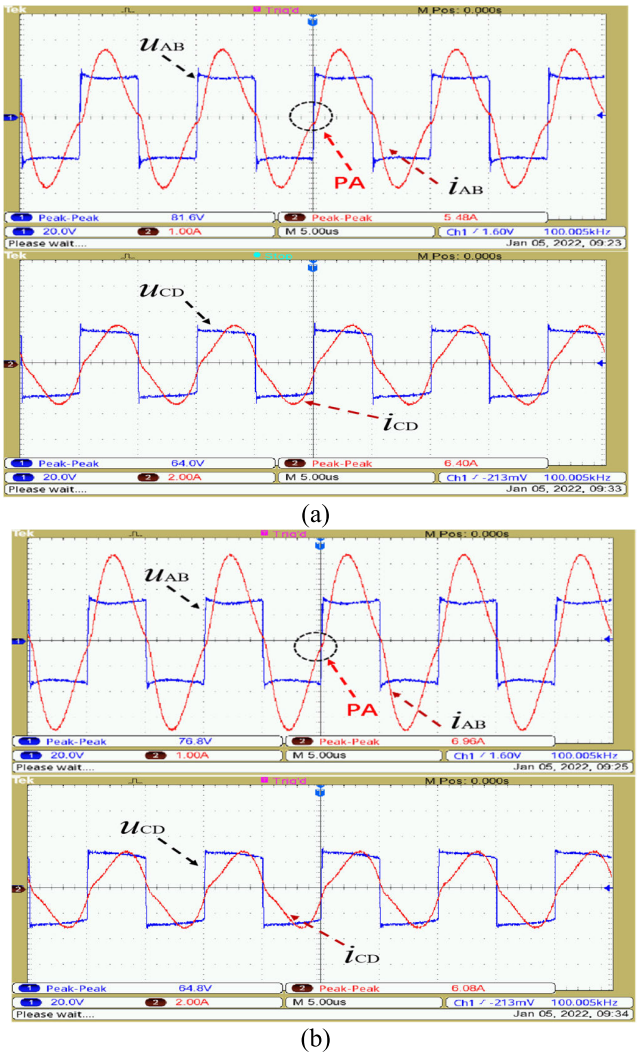

FIGURE 10. Experimental waveforms of uAB, iAB, iCD, and uCD with Rw = 10 Ω. (a) In well-aligned case. (b) 150 mm misalignment in x-axis.

Fig. 10 displays the voltage and current waveforms fed to the rectifier after adjusting the load. If the phase angle (PA) of the voltage and current is the same, then zero voltage switching (ZVS) has been achieved. ZVS indicates that the inverter generates less loss when it is switched on and off. After a 150 mm misalignment along the x-direction, the voltage at the receiver remains nearly unchanged, while the current decreases slightly. As observed from Fig. 10(a) and (b), both positions achieve ZVS, and the voltage amplitude of the receiver hardly changes, demonstrating that the system possesses strong anti-misalignment capability.

The output power of the system is influenced by the mutual coupling of the SQ-BP pad. To corroborate the aforementioned results, Figures 11 and 12 showcase the system's high tolerance for pad misalignment based on experimental and simulation results. Detailed information about the simulation process is provided in Section VII of the Supplementary Document. As previously discussed, the mutual inductance changes significantly along the y-direction. The system can

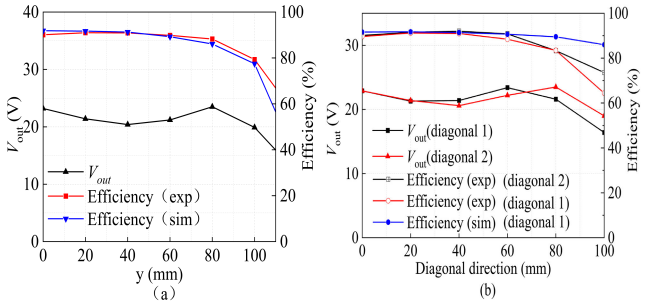

FIGURE 11. Output voltage and efficiency (a) within the y direction misalignment. (b) the diagonal direction misalignment.

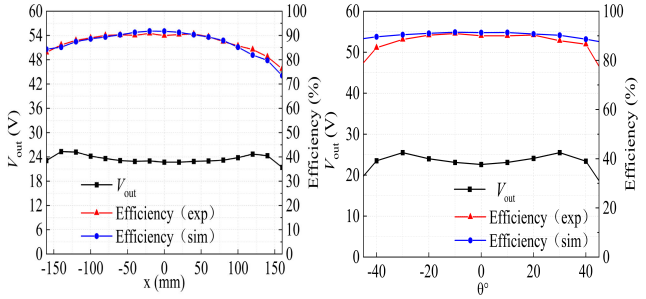

FIGURE 12. Output voltage and efficiency (a) within the *x* direction misalignment. (b) along the rotation angle.

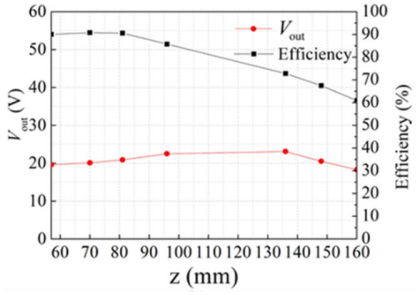

FIGURE 13. Load voltage and efficiency along the *z* direction.

maintain a high output level within a specific range of misalignment due to the compensatory effect of some coils experiencing a decrease in mutual inductance while others experience an increase. Consequently, within the misalignment range of −40 mm to +110 mm in the y-direction, the output voltage and efficiency remain relatively stable, as depicted in Fig. 11(a).

The performance of the proposed SQ-BP structure under diagonal misalignment is depicted in Fig. 11(b). Similar to the changes observed in the y-direction, the system is capable of maintaining a high output voltage and efficiency within a specific misalignment range in the diagonal direction. Since the simulation results for diagonals 1 and 2 are nearly identical, only one set of simulation results is presented. These findings align with the observed changes in mutual inductance and the theoretical analysis.

TABLE 2. Comparison with other methods.

Comparison items	[12]	[46]	[45]	[15]	[16]	[47]	This work
pad size *y*×*x* (mm)	738× 391	900× 1100	738× 391	400× 400	Pad: 400×400 FC: 400×100 ×2	711× 559	Pad: 355 ×290 FC: 500× 250 ×2
Dtx/Drx	1	1	1	1	4	1	1.088
Gap (mm)	120	150	120	150	170	150	60/ 105
Output Power	3.3 kW	15.6 kW	3.3 kW	3.58 kW	500W	3 kW	50W/ 53W
Coupler type (transmitter/ receiver)	Double-D/ Double-D	Asymmetric Coil	Bipolar/ Bipolar	quadruple-D quadrature pads	Quadruple pad/ Quadruple pad	Bipolar/Uniplolar	Solenoid quadrature/Bipolar
Misalignment range (mm) (Misalignment percentage: *y*/ Maximum misalignment in *y* direction, *x*/ Maximum misalignment in *x* direction, *z*/ Maximum gap in *z* direction)	*y*: -80 to +120 (16.3%) *x*: ±160 (40.9%) *z*: ±20 (16.7%)	*x*: ±180 (20%) *y*: ±390 (35.5%) *z*: ±40 (26.7%)	*x*: ±150 (38.4%) *z*: ±20 (16.7%)	*x*: ±150 (37.5%) *y*: ±150 (37.5%) *z*: -20 to +35 (23.3%) diagonal: +100 (17.7%)	*x*: ±200 (50%) *y*: ±170 (42.5%)	*x*: +100(14%) *y*: +150(26.8%)	*x*: ±150 (42.2%)/ ±160 (45%) *z*: +80 (133%)/ -50 to +40 (47.6%) diagonal: ±80 (24.7%) θ : ±40° (22.2%)/ ±45° (25%) *y*: ±90 (31%)
Output fluctuation (%)	5	29	5	5	\	\	*x*, *z*, θ : 6/7 *y* : 10
Efficiency Fluctuation	*y* : 93%-90%	\	*x*: 91.4%- 90.8%	\	*x*: 90.1%-86.2% *y*: 87%-41%	*x*: 93.9%-95.5%% *y*: 94.9%-95.5%	*x*: 90.4%-84.5% *y*: 90.1%-88.2% *z*: 90%-72% diagonal: 90.1%- 84% θ : 89%-86.6%

The load of the system is a resistor whose voltage is in phase with the current. Therefore, the load power can be obtained by measuring the voltage *Vout* at *Rw* and using $Pout = Vout^2/Rw$ after rectifying the output to DC power with a low-loss rectifier. The input power of the system is directly read out by the voltage source SS-6010KD.

Fig. 12 (a) and (b) show the output voltage and efficiency of the proposed system along the x-axis misalignment and the rotational misalignment. Fig. 12 (a) indicates that for a misalignment of −160 mm and +160 mm along the *x*- direction, both the output voltage and efficiency remain relatively stable. The results shown in Fig. 12 (b) demonstrate that the output voltage and efficiency remain relatively stable even for a misalignment of ±40°. This observation is consistent with the findings presented in Fig.S2. In the *z*- direction, the vertical misalignment relies on the complementary characteristics of LCL-S circuit that is insensitive to the mutual inductance changes. This enables the system to maintain a relatively stable output within a certain range. As shown in Fig. 13, the output voltage remains stable and efficiency stays above 80% within the z-misalignment range of 100 mm. More details of the output power are presented in Fig. S18 in the Supplementary Document Section X.

To demonstrate the benefits of the SQ-BP Pad linked to the LCL-S topology, we conducted anti-misalignment experiments at a transmitter-receiver distance of 60 mm and 105 mm, and the results are summarized in Table 2 and compared with other work. Table 2 shows the performance comparison with alternative methods. Compared with methods [12], [45], [47] and [48], our structure has a smaller volume, and the proposed method has especially a better anti-misalignment performance in all directions. In comparison with the methods in [15] and [46], the proposed system has a slightly inferior anti-misalignment performance in *y*- direction, but better performance in *x*- and *y*- directions. Moreover, the proposed approach has a high misalignment tolerance in diagonal and rotation directions. Compared with the method in [16], the proposed system not only has a smaller volume and less magnetic core, but also has a high tolerance to pad misalignment in multiple directions, including diagonal and rotation directions. The results indicate that the

structure has a great potential in low and medium power applications.

IV. CONCLUSION

In this study, a novel hybrid coupler named SQ-BP was introduced to enhance the misalignment tolerance of the IPT in all directions. Compared with the existing magnetic couplers, the SQ-BP coupler improved the misalignment tolerance in horizontal/vertical, diagonal and rotation directions. A misalignment of the secondary side along the x-axis from -150 mm to $+150$ mm and below 80 mm along the z-axis caused a 6% fluctuation in the output voltage. It also achieved an improved misalignment performance in the range of 0 mm to $+80$ mm along the diagonal direction, 0 mm to $+90$ mm in the y-direction, and $-45°$ to $+45°$ along the direction of rotation. Experimental results demonstrated that the new hybrid pad improved the misalignment performance in multi-direction. This designed structure paved the road for utilizing the IPT technology in low and medium power wireless charging for portable mobile devices and unmanned aerial vehicles.

REFERENCES

[1] S. Y. Hui, "Planar wireless charging technology for portable electronic products and Qi," *Proc. IEEE*, vol. 101, no. 6, pp. 1290–1301, Jun. 2013.

[2] Z. Li and L. Li, "A digital twin based real-time parameter identification for mutual inductance and load of wireless power transfer systems," *IEEE Access*, vol. 11, pp. 55404–55412, 2023, doi: 10.1109/ACCESS.2023.3282841.

[3] H. H. Wu, A. Gilchrist, K. D. Sealy, and D. Bronson, "A high efficiency 5 kW inductive charger for EVs using dual side control," *IEEE Trans. Ind. Informat.*, vol. 8, no. 3, pp. 585–595, Aug. 2012, doi: 10.1109/TII.2012.2192283.

[4] Y. Shin, S. Woo, C. Lee, J. Jeong, G. Kwak, and S. Ahn, "Design of a wireless power transfer system with two inputs with large voltage differences for missiles mounted on maritime vessels," *IEEE Access*, vol. 10, pp. 70825–70839, 2022, doi: 10.1109/ACCESS.2022.3187184.

[5] V.-B. Vu, A. Ramezani, A. Triviño, J. M. González-González, N. B. Kadandani, M. Dahidah, V. Pickert, M. Narimani, and J. Aguado, "Operation of inductive charging systems under misalignment conditions: A review for electric vehicles," *IEEE Trans. Transport. Electrific.*, vol. 9, no. 1, pp. 1857–1887, Mar. 2023, doi: 10.1109/TTE.2022.3165465.

[6] P. K. Joseph, D. Elangovan, and P. Sanjeevikumar, "System architecture, design, and optimization of a flexible wireless charger for renewable energy-powered electric bicycles," *IEEE Syst. J.*, vol. 15, no. 2, pp. 2696–2707, Jun. 2021, doi: 10.1109/JSYST.2020.2993054.

[7] T. Diekhans and R. W. De Doncker, "A dual-side controlled inductive power transfer system optimized for large coupling factor variations and partial load," *IEEE Trans. Power Electron.*, vol. 30, no. 11, pp. 6320–6328, Nov. 2015, doi: 10.1109/TPEL.2015.2393912.

[8] Y. Liu, U. K. Madawala, R. Mai, and Z. He, "Zero-phase-angle controlled bidirectional wireless EV charging systems for large coil misalignments," *IEEE Trans. Power Electron.*, vol. 35, no. 5, pp. 5343–5353, May 2020, doi: 10.1109/TPEL.2019.2941709.

[9] J. M. Miller, O. C. Onar, and M. Chinthavali, "Primary-side power flow control of wireless power transfer for electric vehicle charging," *IEEE J. Emerg. Sel. Topics Power Electron.*, vol. 3, no. 1, pp. 147–162, Mar. 2015, doi: 10.1109/JESTPE.2014.2382569.

[10] W. X. Zhong and S. Y. R. Hui, "Maximum energy efficiency tracking for wireless power transfer systems," *IEEE Trans. Power Electron.*, vol. 30, no. 7, pp. 4025–4034, Jul. 2015, doi: 10.1109/TPEL.2014.2351496.

[11] M. Fu, H. Yin, X. Zhu, and C. Ma, "Analysis and tracking of optimal load in wireless power transfer systems," *IEEE Trans. Power Electron.*, vol. 30, no. 7, pp. 3952–3963, Jul. 2015, doi: 10.1109/TPEL.2014.2347071.

[12] L. Zhao, D. J. Thrimawithana, U. K. Madawala, A. P. Hu, and C. C. Mi, "A misalignment-tolerant series-hybrid wireless EV charging system with integrated magnetics," *IEEE Trans. Power Electron.*, vol. 34, no. 2, pp. 1276–1285, Feb. 2019, doi: 10.1109/TPEL.2018.2828841.

[13] Y. Chen, B. Yang, Z. Kou, Z. He, G. Cao, and R. Mai, "Hybrid and reconfigurable IPT systems with high-misalignment tolerance for constant-current and constant-voltage battery charging," *IEEE Trans. Power Electron.*, vol. 33, no. 10, pp. 8259–8269, Oct. 2018, doi: 10.1109/TPEL.2018.2809785.

[14] X. Qu, Y. Yao, D. Wang, S.-C. Wong, and C. K. Tse, "A family of hybrid IPT topologies with near load-independent output and high tolerance to pad misalignment," *IEEE Trans. Power Electron.*, vol. 35, no. 7, pp. 6867–6877, Jul. 2020, doi: 10.1109/TPEL.2019.2955299.

[15] Y. Chen, B. Yang, X. Zhou, Q. Li, Z. He, R. Mai, and J.-S. Lai, "A hybrid inductive power transfer system with misalignment tolerance using quadruple-D quadrature pads," *IEEE Trans. Power Electron.*, vol. 35, no. 6, pp. 6039–6049, Jun. 2020, doi: 10.1109/TPEL.2019.2954906.

[16] Y. Yao, S. Gao, Y. Wang, X. Liu, X. Zhang, and D. Xu, "Design and optimization of an electric vehicle wireless charging system using interleaved boost converter and flat solenoid coupler," *IEEE Trans. Power Electron.*, vol. 36, no. 4, pp. 3894–3908, Apr. 2021, doi: 10.1109/TPEL.2020.3019441.

[17] Y. Yao, S. Gao, Y. Wang, S. Zhang, X. Liu, and D. Xu, "A comparison study between flat solenoid coupler and planar square coupler for WPT systems," in *Proc. 45th Annu. Conf. IEEE Ind. Electron. Soc.*, vol. 1, Oct. 2019, pp. 3431–3435.

[18] M. Budhia, J. T. Boys, G. A. Covic, and C.-Y. Huang, "Development of a single-sided flux magnetic coupler for electric vehicle IPT charging systems," *IEEE Trans. Ind. Electron.*, vol. 60, no. 1, pp. 318–328, Jan. 2013, doi: 10.1109/TIE.2011.2179274.

[19] A. Zaheer, G. A. Covic, and D. Kacprzak, "A bipolar pad in a 10-kHz 300-W distributed IPT system for AGV applications," *IEEE Trans. Ind. Electron.*, vol. 61, no. 7, pp. 3288–3301, Jul. 2014, doi: 10.1109/TIE.2013.2281167.

[20] Y. Nagatsuka, N. Ehara, Y. Kaneko, S. Abe, and T. Yasuda, "Compact contactless power transfer system for electric vehicles," in *Proc. Int. Power Electron. Conf. (ECCE ASIA)*, Jun. 2010, pp. 807–813.

[21] Y. Yao, S. Gao, J. Mai, X. Liu, X. Zhang, and D. Xu, "A novel misalignment tolerant magnetic coupler for electric vehicle wireless charging," *IEEE J. Emerg. Sel. Topics Ind. Electron.*, vol. 3, no. 2, pp. 219–229, Apr. 2022, doi: 10.1109/JESTIE.2021.3051550.

[22] M. Budhia, G. Covic, and J. Boys, "A new IPT magnetic coupler for electric vehicle charging systems," in *Proc. 36th Annu. Conf. IEEE Ind. Electron. Soc.*, Nov. 2010, pp. 2487–2492.

[23] G. Yang, C. Zhu, K. Song, K. Liu, R. Lu, and G. Wei, "Power stability optimization method of wireless power transfer system against wide misalignment," in *Proc. IEEE Transp. Electrific. Conf. Expo, Asia–Pacific (ITEC Asia–Pacific)*, Aug. 2017, pp. 1–6.

[24] B. Kallel, O. Kanoun, and H. Trabelsi, "Large air gap misalignment tolerable multi-coil inductive power transfer for wireless sensors," *IET Power Electron.*, vol. 9, no. 8, pp. 1768–1774, Jun. 2016, doi: 10.1049/iet-pel.2015.0800.

[25] C. Sritongon et al., "Novel IPT multi-transmitter coils with increased misalignment tolerance and system efficiency," in *Proc. IEEE Int. Symp. Circuits Syst.*, 2018, pp. 1–5.

[26] Z. Dang, Y. Cao, and J. A. Abu Qahouq, "Reconfigurable magnetic resonance-coupled wireless power transfer system," *IEEE Trans. Power Electron.*, vol. 30, no. 11, pp. 6057–6069, Nov. 2015, doi: 10.1109/TPEL.2015.2422776.

[27] Y. Cao and J. A. Abu Qahouq, "Modelling and control design of reconfigurable wireless power transfer system for transmission efficiency maximisation and output voltage regulation," *IET Power Electron.*, vol. 12, no. 8, pp. 1903–1916, Jun. 2019, doi: 10.1049/iet-pel.2018.6207.

[28] Z. Yuan, M. Saeedifard, C. Cai, Q. Yang, P. Zhang, and H. Lin, "A misalignment tolerant design for a dual-coupled LCC-S-compensated WPT system with load-independent CC output," *IEEE Trans. Power Electron.*, vol. 37, no. 6, pp. 7480–7492, Jun. 2022, doi: 10.1109/TPEL.2022.3141453.

[29] Z. Li and Y. Liu, "Orthogonal laminated magnetic integrated coupler for the wireless charging system with multiple power transfer channels," *IET Power Electron.*, vol. 13, no. 12, pp. 2523–2530, Aug. 2020, doi: 10.1049/iet-pel.2019.1315.

[30] M. Chigira, Y. Nagatsuka, Y. Kaneko, S. Abe, T. Yasuda, and A. Suzuki, "Small-size light-weight transformer with new core structure for contactless electric vehicle power transfer system," in *Proc. IEEE Energy Convers. Congr. Expo.*, Sep. 2011, pp. 260–266.

[31] H. Takanashi, Y. Sato, Y. Kaneko, S. Abe, and T. Yasuda, "A large air gap 3 kW wireless power transfer system for electric vehicles," in *Proc. IEEE Energy Convers. Congr. Expo. (ECCE)*, Sep. 2012, pp. 269–274.

[32] T. Fujita, T. Yasuda, and H. Akagi, "A wireless power transfer system with a double-current rectifier for EVs," in *Proc. IEEE Energy Convers. Congr. Expo. (ECCE)*, Sep. 2016, pp. 1–7.

[33] G. Yang, S. Dong, C. Zhu, R. Lu, G. Wei, and K. Song, "Design of a high lateral misalignment tolerance magnetic coupler for wireless power transfer systems," in *Proc. IEEE PELS Workshop Emerg. Technol., Wireless Power Transf. (WoW)*. Union City, NJ, USA: Wire, May 2017, pp. 34–39.

[34] Y. Tang, F. Zhu, Y. Wang, and H. Ma, "Design and optimizations of solenoid magnetic structure for inductive power transfer in EV applications," in *Proc. 41st Annu. Conf. IEEE Ind. Electron. Soc.*, Nov. 2015, pp. 001459–001464.

[35] M. Eladawy and I. A. Metwally, "Performance improvement of different resonant inductive couplers used for wireless power transfer," *IEEE Sensors J.*, vol. 23, no. 12, pp. 12936–12946, Jun. 15, 2023, doi: 10.1109/JSEN.2023.3269346.

[36] L. Chen, C. Zhang, T. Ben, and H. Nie, "Design and optimization of a magnetic coupling structure with high anti-offset for wireless power transfer," *J. Electr. Eng. Technol.*, vol. 18, no. 2, pp. 1083–1098, Jul. 2022, doi: 10.1007/s42835-022-01170-8.

[37] H. Li, M. Liu, L. Kong, and Y. Wang, "An independent dual-coil driving topology for wireless power transfer," *IEEE Trans. Power Electron.*, vol. 38, no. 2, pp. 1378–1383, Feb. 2023, doi: 10.1109/TPEL.2022.3208020.

[38] Y. Li, T. Lin, R. Mai, L. Huang, and Z. He, "Compact double-sided decoupled coils-based WPT systems for high-power applications: Analysis, design, and experimental verification," *IEEE Trans. Transport. Electrific.*, vol. 4, no. 1, pp. 64–75, Mar. 2018, doi: 10.1109/TTE.2017.2745681.

[39] T. Mei, X. Zhang, F. Liu, X. Chen, and R. M. Kennel, "Multi-frequency phase-shifted angle control strategy for a two-phase MCR WPT system with multiple loads to achieve targeted power distribution and stable transmission power," in *Proc. IEEE Appl. Power Electron. Conf. Expo. (APEC)*, Mar. 2019, pp. 3117–3122.

[40] X.-J. Ge, Y. Sun, Z.-H. Wang, and C.-S. Tang, "Dual-independent-output inverter for dynamic wireless power transfer system," *IEEE Access*, vol. 7, pp. 107320–107333, 2019, doi: 10.1109/ACCESS.2019.2933017.

[41] X. Wang, J. Xu, H. Ma, and P. Yang, "A high efficiency LCC-S compensated WPT system with dual decoupled receive coils and cascaded PWM regulator," *IEEE Trans. Circuits Syst. II, Exp. Briefs*, vol. 67, no. 12, pp. 3142–3146, Dec. 2020, doi: 10.1109/TCSII.2020.2973770.

[42] Z. Hao, P. Fu, and P. Cao, "A new hybrid magnetic coupler for large misalignment tolerance in inductive power transfer system," *J. Phys., Conf. Ser.*, vol. 2108, no. 1, Nov. 2021, Art. no. 012080.

[43] H.-E. Committee, "Wireless power transfer for light-duty plug-in/electric vehicles and alignment methodology," SAE Tech. Paper J2954_202010, Apr. 2019.

[44] A. Ahmad, M. S. Alam, and A. A. S. Mohamed, "Design and interoperability analysis of quadruple pad structure for electric vehicle wireless charging application," *IEEE Trans. Transport. Electrific.*, vol. 5, no. 4, pp. 934–945, Dec. 2019, doi: 10.1109/TTE.2019.2929443.

[45] L. Zhao, D. J. Thrimawithana, and U. K. Madawala, "Hybrid bidirectional wireless EV charging system tolerant to pad misalignment," *IEEE Trans. Ind. Electron.*, vol. 64, no. 9, pp. 7079–7086, Sep. 2017, doi: 10.1109/TIE.2017.2686301.

[46] S. Y. Choi, J. Huh, W. Y. Lee, and C. T. Rim, "Asymmetric coil sets for wireless stationary EV chargers with large lateral tolerance by dominant field analysis," *IEEE Trans. Power Electron.*, vol. 29, no. 12, pp. 6406–6420, Dec. 2014, doi: 10.1109/TPEL.2014.2305172.

[47] T. Kan, T.-D. Nguyen, J. C. White, R. K. Malhan, and C. C. Mi, "A new integration method for an electric vehicle wireless charging system using LCC compensation topology: Analysis and design," *IEEE Trans. Power Electron.*, vol. 32, no. 2, pp. 1638–1650, Feb. 2017, doi: 10.1109/TPEL.2016.2552060.

[48] H. Le-Huu and C. Seo, "A hybrid transmitting coil for improving angular freedom of a wireless power transfer system," *IEEE Microw. Wireless Technol. Lett.*, vol. 34, no. 1, pp. 119–122, Jan. 2024, doi: 10.1109/LMWT.2023.3337548.

PENGFEI CAO (Member, IEEE) received the Ph.D. degree from Lanzhou University, Lanzhou. He is currently an Associate Professor with Lanzhou University. He has published more than 20 papers in journals and international refereed conferences. His research interests include magnetically coupled wireless energy transmission and the optimization of coil topology.

JIQIANG SHANG was born in Dingxi, Gansu, China, in 1999. He received the bachelor's degree in automation from Henan University, China, in 2023. He is currently pursuing the master's degree in communications with Lanzhou University, China. His research interests include wireless energy transmission and coil design.

ZHENGNAN YUAN was born in Xiangyang, Hubei, China, in 1985. He received the B.S. degree in physics from Lanzhou University in 2007, and he is an on-the-job master degree candidate of Lanzhou University. He is currently working in Lanzhou Institute of Physics (Lanzhou, China), and has been engaged in the research and industrial development of electric vacuum products since 2007.

MING SONG was born in Huanggang, Hubei, China, in 1999. He received the bachelor's degree in communication engineering from Hubei University, China, in 2021. He is currently pursuing the master's degree in communications with Lanzhou University, China. His research interests include wireless energy transmission and coil design.

CONGCONG LI was born in Qingyang, Gansu, China, in 1999. He received the bachelor's degree in communication engineering from the Huazhong University of Science and Technology, China, in 2021. He is currently pursuing the master's degree in communications with Lanzhou University, China. His research interests include wireless energy transmission and frequency compensation.

PENGCHENG FU received the bachelor's degree from Lanzhou University, Lanzhou, where he is currently pursuing the master's degree. His research interests include wireless energy transmission and frequency compensation.

ZHONGXIU HAO received the B.S. degree from Lanzhou University, Lanzhou, China, where she is currently pursuing the M.S. degree. Her main research interest includes wireless power transfer.

YONG YANG received the bachelor's degree from Guilin Institute of Technology and the master's degree from Lanzhou University. He is currently with the Department of Industry and Information Technology of Gansu Province. His research interest includes wireless power transfer.

ANZONG HU received the bachelor's degree from Gansu University of Technology, Lanzhou. He is currently with Lanzhou Huayu Aerospace Service Guarantee Company Ltd. His research interest includes wireless power transfer.